Characterization of cisplatin loaded hydrophilic glycol chitosan modified eumelanin nanoparticles for potential controlled-release application

Aleyna Atik [a], Tuğçe Günal [a], Pınar Acar Bozkurt [b], Sıla Naz Köse [c], Burcak Alp [d], Cihangir Yandım [c], Nurettin Mete Kaleli [b], Gözde Kabay [e,**], Gizem Kaleli-Can [a,*]

[a] Department of Biomedical Engineering, İzmir Democracy University, Izmir, 35140, Turkey
[b] Department of Chemistry, Science Faculty, Ankara University, Ankara, 06100, Turkey
[c] Department of Genetics and Bioengineering, Faculty of Engineering, Izmir University of Economics, Izmir, 35330, Turkey
[d] Department of Biomedical Engineering, İzmir University of Economics, Izmir, 35330, Turkey
[e] Institute of Functional Interfaces - IFG, Karlsruhe Institute of Technology, Karlsruhe, 76344, Germany

ARTICLE INFO

Keywords:
Natural melanin nanoparticles
Eumelanin
Glycol chitosan
Cisplatin
Nanoparticle drug delivery
Super Case II Transport

ABSTRACT

Free liquid cytotoxic substances, such as cisplatin (CDDP), have been widely administered for the conventional chemotherapy treatment of cancer patients. However, this classical approach has several drawbacks, including high dosage requirements, poor bioavailability, low therapeutic index, and geno-/cyto-toxicity resulting in several adverse side effects that constrain patient compliance and clinical outcomes. Such downsides can be improved by replacing conventional drugs with advanced nanocomposite-drug conjugates. In line with this, our study aimed to characterize a novel potential drug nano delivery system, so-called hydrophilic glycol chitosan (HGC) coated melanin nanoparticles (MNPs), to improve the abovementioned constraints in the case of classical chemotherapy drug cisplatin. Following the production of MNP-based nanocomplexes by a single-step mixing, essential physical and chemical characterizations were performed. The nanoformulations generated here were spherically shaped with an optimum size range (between 100 and 200 nm) and exhibited comparable drug loading capacities (21.7% ± 0.5 for the CDDP-MNPs and 24.7% ± 0.4 for HGC/CDDP-MNPs) and remarkable entrapment efficiencies (93.2% ± 2.0 for CDDP-MNPs and 94.9% ± 1.1 for HGC/CDDP-MNPs) as a biopolymer. Notably, the cell viability assay showed that MNP-based nanocarriers could inhibit the proliferation of liver cancer cells in a more prolonged fashion compared to free CDDP. The TGA and FTIR-ATR analyses confirmed the compatibility between CDDP and its nanocarrier MNP. The Super Case II Transport was primarily in charge of controlling CDDP release from both matrices as a result of polymer relaxation and swelling of HGC-CDDP-MNPs and CDDP-MNPs, which is highly preferred because it enables simple manipulation of the nanocarrier properties to suit the disease biology. All of these findings point to the natural MNP-based nanoformulation's superiority as a prospective and cutting-edge chemotherapeutic nano-delivery technology.

1. Introduction

Cancer is the universal cause of death worldwide, and about 30.2 million new cases are estimated to be diagnosed by 2040 [1]. Due to the high prevalence of this condition, extensive effort has been put into improving existing cancer management strategies for facilitating all stages of cancer diagnosis, site-specific screening, and therapy.

Surgery, chemotherapy, and radiotherapy are routinely used in conventional cancer therapy [2]. While surgical removal of the tumors is an effective option only at the early cancer stages; radiation therapy damages healthy cells, organs, and tissues. Even though chemotherapy reduces morbidity and mortality by killing fast-growing cancer cells, such treatment can cause several adverse side effects because of damaging healthy cells while traveling throughout the body [3]. For instance, *cis*-diamminedichloridoplatinum(II) (CDDP) is a potent and extensively used chemotherapeutic agent owing to its broad-spectrum antitumor activity against solid neoplasms by leading to cell apoptosis [4–7]. It has been broadly applied for several advanced cancer

* Corresponding author.
** Corresponding author.
E-mail addresses: gozde.kabay@kit.edu (G. Kabay), gizem.kalelican@idu.edu.tr (G. Kaleli-Can).

treatments (i.e., breast, bladder, ovaries, and testicles) through intravenous administration of its free liquid dosage formulation [7–9], which may cause several complications (i.e., fatigue, nausea, hair, and weight loss) [9,10]. In addition to its cyto-, geno-toxicity [5,11,12], the drug resistance [13] acquired by the cancer cells evades the efficacy and bioavailability of CDDP-based chemotherapy, limiting its sole usage. Although combinatory therapeutic strategies [4,7] were established to minimize the drawbacks of CDDP and its several counterparts, these approaches still yield overall clinical performance [7].

Alternatively, nanomedicine offers advanced nanoformulations and has the power to revolutionize cancer management by limiting the high dose requirements, enabling the controlled release of chemotherapeutics with improved bioavailability, and aiding patient compliance by eliminating side effects [14–19]. So far, several chemotherapeutics combined with liposomal [20], metallic [21,22], ceramic [23], bio-, and synthetic-polymer [24,25] nanocarriers have been utilized to localize drugs at the cancer site and to lower systemic toxicity, adverse side effects, and drug resistance. Among all, materials of biological origin are

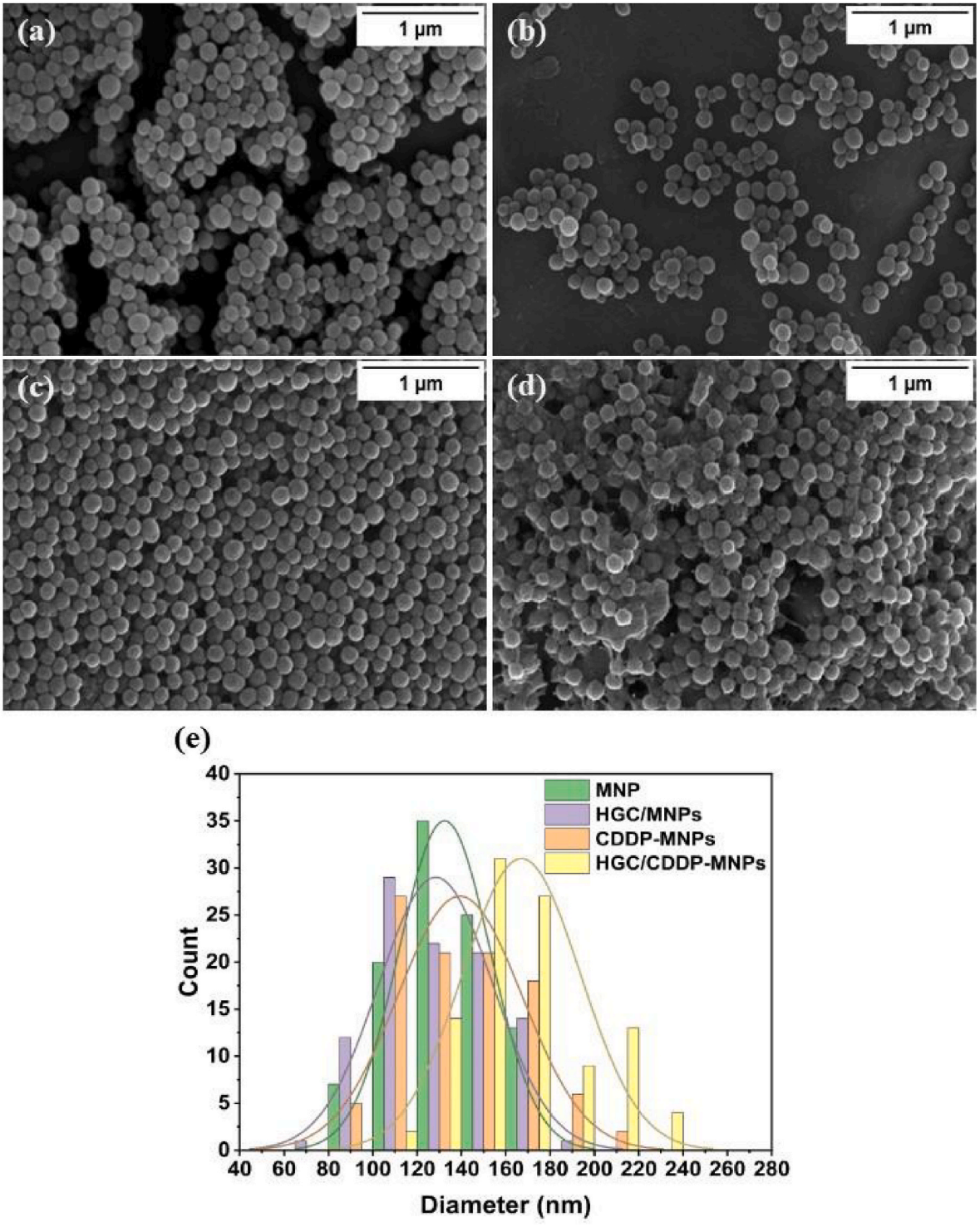

Fig. 1. SEM images of MNPs (a), CDDP-MNPs (b), HGC/MNPs (c) HGC/CDDP-MNPs (d), and their associated particle size distribution graph (n 100) (e). The original magnification of the SEM images taken was 100,0000x. For data evaluation and statistical analyses, OriginLab© software was used.

exceedingly demanded as nanocarriers due to their versatile features, including biocompatibility, biodegradability, low cyto-, geno-toxicity, and sustainability [26,27]. However, several issues related to scaling up, low drug-loading capacity, and wide size distribution remain challenging [26,28].

In line with this, melanin nanoparticles (MNPs) extracted from natural resources [29,30] have gained increasing attention as sustainable nanocarriers not only because of the biocompatibility but also because of the added features such as radical scavenging [31], antioxidant activity [32,33], and mainly, intrinsic photoacoustic properties and metal chelation [34,35], which facilitates efficient prognosis through simultaneous site-specific imaging and therapy. Furthermore, MNPs *per se* do not have any cytotoxic effect on healthy fibroblast cells [36]. Despite various advantages of MNPs, they are subjected to aggregation and low solubility in physiological conditions, which severely limited their application in drug loading and biomedical application [37]. Thus, surface modification of natural MNPs is needed. Lately, the method of layer-by-layer technique that allows modification via electrostatic attractions between opposite charges on the surface of each component has generated great interest with its ease of apply [34]. Although the layer-by-layer technique has been reported for the polyvinyl alcohol-MNPs and glycol chitosan-MNPs couples [34,38], these interactions were mainly focused on the thin film production not the surface tailoring of nanoparticles. In line with this, for the first time, surface coatings of negatively charged melanin nanoparticle-based drug delivery systems with positively charged glycolic chitosan which is also cell friendly and not cytotoxic [39,40] were studied.

In this study, we developed a natural melanin-based cisplatin nanocomplex (CDDP-MNPs) by tailoring nanocarrier surfaces with hydrophilic glycol chitosan (HGC) with a layer-by-layer technique. The sustainable nanoformulation herein has a comparable drug loading performance (25%) to synthetic MNPs published in our previous finding [28] (35%) and other studies utilizing natural melanin nanocarriers [41,42]. In addition, achieving HGC coating resulted in a more sustained and prolonged release of the loaded cisplatin without cytotoxicity than its free form, suggesting that the developed nano-chemotherapeutic formulation can be a safe alternative to its conventional counterpart for further clinical applications that prioritize nanomedicine-mediated effective cancer treatments.

2. Experimental

2.1. Materials

Food-grade cuttlefish ink paste was obtained from Nortindal Sea Products Ltd. (Guipúzcoa, Spain). Hydrophilic glycol chitosan (MW: 190–310 KDa), acetic acid, ortho-phenylene diamine (o-phenylenediamine, OPDA), dimethylformamide (DMF), and phosphate buffer saline (PBS, pH: 7.4, 0.01 M) were purchased from Merck (St. Louis, MO, USA). Cisplatin (CDDP, 50 mg/100 mL) was commercially obtained from Koçak Farma (Istanbul, Turkey). CDDP was stored in DIW containing sodium hydroxide (NaOH) and dilution of the drug was performed with saline solution. All solutions were prepared with (Millipore Corp., Bedford, MA, USA) deionized water (DIW, 18.2 MΩ cm ^{1}).

2.2. Preparation of melanin nanoparticles

Natural melanin nanoparticles (MNPs) were extracted from commercially available *Sepia Officinalis* ink paste following a previous method [43]. First, the ink paste was diluted using DIW, and the suspension was centrifuged at 10,000 rpm for 20 min. The supernatant was removed, and the obtained pellet was washed with DIW. This process was repeated five times to remove salt and impurities. Then, the final pellets were dried in the vacuum oven (MIPROLAB, Turkey) at 50 °C for 48 h [30]. The collected melanin powders were dispersed in 10 mL of DIW to procure 5% (w:v) of colloidal MNP suspension and stored at room temperature (25 °C) to be used for further experiments.

2.3. Chemotherapeutic drug loading

The CDDP conjugation to the MNPs was achieved via single-step mixing. First, 1 mL of CDDP was mixed with 2 mL of MNPs suspension and stirred for 24 h with a magnetic stirrer. Then, the mixture was centrifuged at 10,000 rpm for 20 min, and CDDP-MNPs were obtained.

Next, hydrophilic glycol chitosan (HGC) modification was achieved for increased bioavailability of CDDP-MNPs following a previous method [44]. Briefly, 1% (w:v) CDDP-MNPs were mixed with the chitosan solution (1% w:v) and centrifuged (5000 rpm, 15 min) to acquire HGC/CDDP-MNPs. The supernatants were collected and stored at 4 °C until further analyses were carried out. To remove excessive substances on the MNPs' surface, the modified samples were washed three times with DIW.

2.4. Drug loading capacity and entrapment efficiency

Cisplatin has a low molar absorptivity in the UV region of the electromagnetic spectrum [45]. However, it consists of platinum (Pt) that can be tracked in the visible range upon reaction with o-phenylenediamine (OPDA) in the presence of dimethylformamide (DMF) at pH 6.8. Using the maximum absorption peak obtained at 704 nm by UV–vis spectroscopy device (UV–1280, Shimadzu Corp., Kyoto, Japan), a calibration curve (Fig. S1) was plotted using the absorbance data obtained for various CDDP concentrations (Supplementary Material). To determine the exact CDDP concentration within produced CDDP-conjugated nanoformulations (CDDP-MNPs, HGC/CDDP-MNPs), 1 mL of the supernatant was taken and mixed with an equal volume of OPDA solution (1.2 mg/mL in DMF). Then, the mixture was heated in a 100 °C water bath for 10 min before recording the absorbance values. Due to the possibility of interference that an MNPs leakage can cause, the baseline correction was applied at 600 and 800 nm absorbance values. The drug entrapment efficiency **(Equation (1))** and the loading capacity **(Equation (2))** of each nanoformulation were calculated using the following equations:

$$\textit{Entrapment efficiency}\ (\%) = \frac{\textit{The total amount of CDDP} \quad \textit{Free amount of CDDP}}{\textit{The total amount of CDDP}}\ x\ 100 \tag{1}$$

$$\textit{Loading capacity}\ (\%) = \frac{\textit{The total amount of CDDP} \quad \textit{Free amount of CDDP}}{\textit{Weight of MNPs}}\ x\ 100 \tag{2}$$

2.5. Characterization of nanoparticles

Scanning electron microscopy (SEM, FEI Quanta 400F, Hillsboro, OR, USA) was performed for the morphological characterization of the MNPs, HGC/MNPs, CDDP-MNPs, and HGC/CDDP-MNPs. Before the

examination, the samples were sputter-coated with a gold-palladium (Au–Pd) mixture, and the SEM images were taken at a 7.5 kV accelerating voltage. The average nanoparticle diameter for each formulation was determined by measuring the particle diameters from the collected SEM images using ImageJ® software (NIH, MD, USA). All data presented as the mean ± SD (n = 100).

The chemical groups on the produced particles (MNPs, CDDP, CDDP-MNPs, HGC/MNPs, HGC/CDDP-MNPs) and possible interaction between components were characterized using attenuated total reflectance Fourier transform infrared spectroscopy (ATR-FTIR) device (PerkinElmer Spectrum Two, Waltham, MH, USA), and performed within a wavenumber range of 4000 1000 cm ^{1}.

Thermal characteristics and the compatibility between components of nanocomplexes were examined using thermal gravimetric analysis (TGA, TA Instruments Co., DE, USA). Samples weighed about 5 mg were placed into aluminum pans and heated from 30 to 600 °C at a heating rate of 10 °C/min under an inert nitrogen atmosphere.

2.6. In vitro drug release

The *in vitro* drug release of CDDP from CDDP-MNPs and HGC/CDDP-MNPs was evaluated in physiologic buffer (PBS, pH: 7.4). Briefly, all MNP formulations (MNP, HGC/MNPs, and HGC/CDDP-MNPs) were resuspended in PBS (pH: 7.4, 1 mg/mL) and incubated at 37 °C at 300 rpm speed. At predetermined time points, 1 mL of samples were collected and then centrifuged (10,000 rpm for 20 min). The released concentration of CDDP in the collected supernatants was measured at 704 nm wavelength using a UV–vis spectrophotometer.

To evaluate the mechanism of the CDDP release from prepared nanoformulations, obtained release data were fitted to four distinct kinetic models: zero-order, first-order, simplified Higuchi, and Korsmeyer-Peppas. A more detailed explanation of these kinetic models and their respected equations are given in the Supplementary Material. The data were shown as the mean ± SD of three replicated measurements for each nanoformulation. OriginLab© software was used to evaluate repeated measures using a multivariate approach (multivariate analysis of variance, MANOVA). The data are summarized numerically, and 95% confidence intervals for the differences in the mean dissolution profiles at each dissolution time point are evaluated [46,47].

2.7. In vitro cytotoxicity assay

The *in vitro* cytotoxicity effect of each nanoformulation was tested by subjecting them to the hepatocarcinoma cell line (Huh7). For the MTT assay [48], the cells were seeded in 96-well plates containing 100 μL of DMEM low glucose medium supplemented with 10% FCS, 50 units/mL penicillin, and 50 μg/mL streptomycin. The cellular density was adjusted to be 5000 cells per well (n = 3). After cell seeding, the medium was replaced with a fresh medium containing the drug and incubated overnight. In detail, 15 μL of MTT solution (5 mg/mL, BioBasic-0793) was supplied to each well, and the cells were further incubated at 37 °C for 4 h. To dissolve the formazan crystals, 100 μL of DMSO was added after removing all media, and the absorbance values were recorded at 570 nm using a microplate reader (Multiskan FC, ThermoFisher Sci., Waltham, MA, USA). Furthermore, cell viability, proliferation, and toxicity that varied after subjecting with various free and nanocarrier-bound drug concentrations (0.1, 0.3, 0.5, 1, 2.5, 5, and 10 μg/mL) for 72 h were investigated.

3. Results and discussion

3.1. Characterization of nanoparticles

The size and shape of nanoparticles are critical for obtaining a controlled release profile of the loaded drug within the nanoformulation [49,50]. In a physiological environment, nanoparticles smaller than 10 nm were excreted by renal clearance, and those larger than 300 nm were caught by the components of the reticuloendothelial system [50,51]. Additionally, the nanoparticles sized within the 100–200 nm range could escape from phagocytosis, enhancing their circulation and retention time within the physiological environment, resulting in increased bioavailability. On the other hand, rigid and spherical nanoparticles have shown a shorter blood circulation time but are highly uptaken by tumor cells compared to elongated and soft particles [52]. For that reason, the spherical-shaped nanoparticles having a size of 100–200 nm have been accepted as an optimum for enhanced therapeutic efficacy [53].

SEM analyses were conducted to evaluate the prepared nanoformulations' morphological structure and their related size distribution. The SEM images revealed that MNPs with uniform spherical shapes having an average size of 132 ± 18 nm (Fig. 1a) were produced. Upon CDDP loading and solely HGC coating, the mean diameters were not altered significantly and were calculated as 128 ± 22 nm and 139 ± 23 nm (Fig. 1b and c). On the contrary, a slight increment in particle diameter was observed (167 ± 26 nm) upon HGC-conjugation to the CDDP-MNPs (Fig. 1d). Moreover, produced particles were spherically shaped, and the mean diameters were smaller than 200 nm, satisfying optimum shape/diameter needs for an increased bioavailability when applied *in vivo*.

3.2. Drug compatibility analyses

The compatibility between drugs and nanoparticles forming nanodrug formulations is essential to minimize the burst release [54]. Therefore, the ATR-FTIR spectrum analyses of each component (Fig. 2a) and their produced nanoformulations were carried out as sketched in Fig. 2b. Firstly, the spectrum of MNPs was obtained. A broad peak from 3620 cm ^{1} to 2660 cm ^{1} comes from –OH and NH_2 vibrations from the carboxylic acid and phenolic and aromatic amino functions in the indolic and pyrrolic systems. Additionally, bands at 2920 cm ^{1} (the stretching of –CH band), 1630 cm ^{1} (the stretching of C═O in COO , quinone, or ketone), 1453 cm ^{1} (the vibration of C═C aromatic ring vibration/the symmetric stretching of COO) and 1388 cm ^{1} (the stretching of pyrrole ring), 1248 cm ^{1} (CH in-plane deformation) and 1164 cm ^{1} (pyrrole –NH in-plane deformation/ring breathing) were detected. In the spectrum of hydrophilic glycol chitosan, a broad peak was observed at 3310 cm ^{1}, indicating –OH and NH_2 stretching. The C═O stretching of the acetyl group (amide-I) band was seen at 1642 cm ^{1} [44,55,56]. After HGC coating of MNPs, the intensity decrement of the –OH stretching band and a shift on the primary amine band (amide-II) from 1642 to 1526 cm ^{1} were formed. These changes could be linked to the hydrogen bond formation or secondary interactions between the –OH (MNPs) and NH_2 groups (chitosan) in π-conjugated structures (i.e., dihydroxyindole, indolequinone) [57,58].

In the CDDP spectrum, the broadband at 3500 cm ^{1}– 3000 cm ^{1} indicates formation of aquated CDDP because of the –OH stretching and the sharp peak at 1637 cm ^{1} (C═O) disguised the amine peaks of the CDDP. After the CDDP was conjugated with MNPs, the peaks arose at 3310 cm ^{1} and 1635 cm ^{1}, indicating O–H and –C═O stretching of the acetyl group (amide-I) [44]. The carboxylate peak at 1630 cm ^{1} were shifted to 1635 cm ^{1}. This shift could be arisen from the linkage between carboxylated and platinum hydroxide of aquated cisplatin [59–61]. Following HGC coating, the physical interaction (H-bonding or van der Waals force) between HGC and the remaining functional sides of CDDP-MNPs after CDDP interaction caused a large shift of carboxylate peak (14 cm ^{1}) [44].

The thermal behavior of the nanocomplexes and their forming constituents were investigated with TGA to evaluate the possible interaction between components when heated each up to 600 °C. At first, the building block powders used to construct nanocarrier systems were analyzed. As shown in Fig. 2c, the thermogravimetric spectrum of CDDP showed a single-step decomposition at 92 °C with a total weight loss of

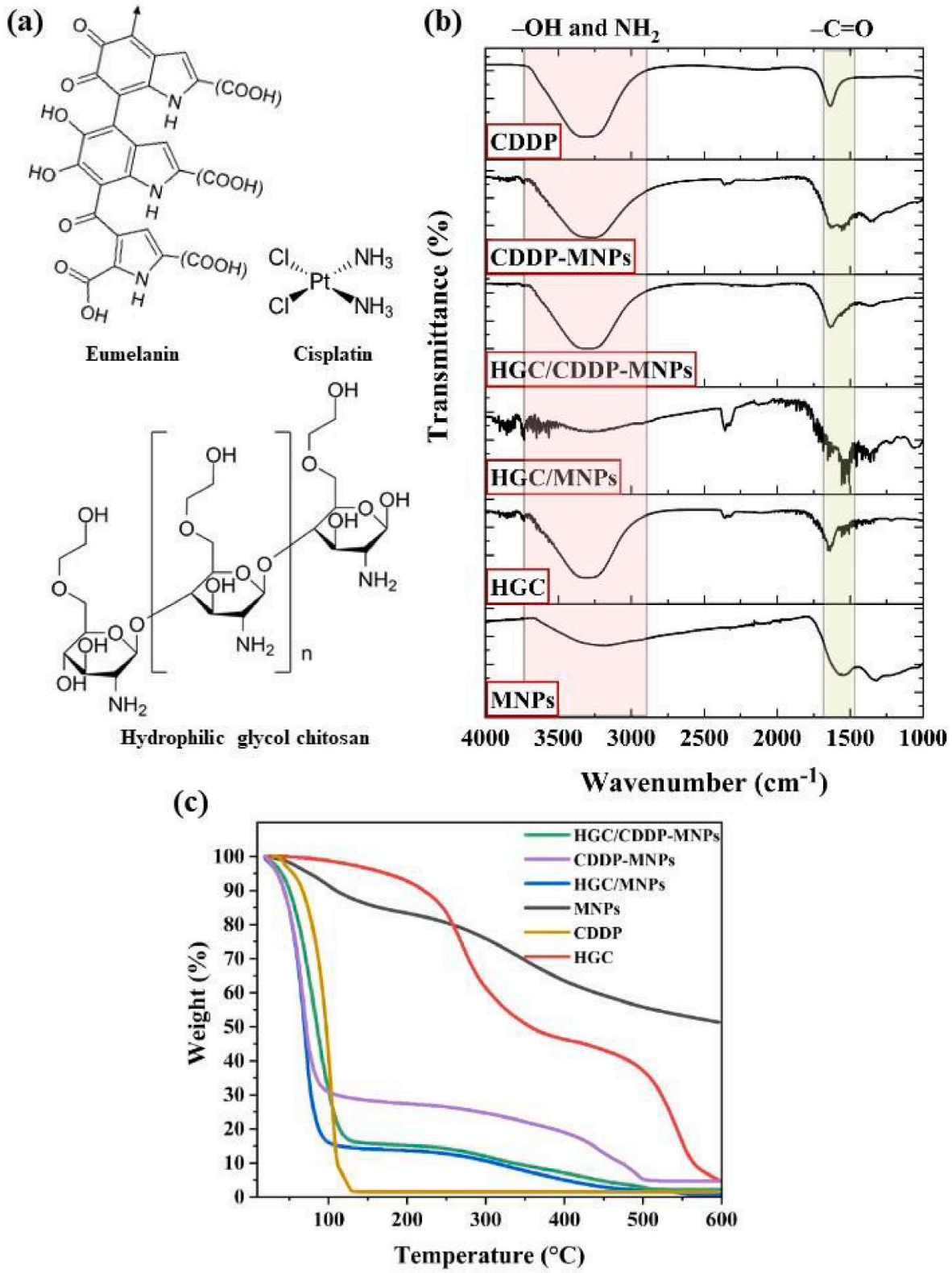

Fig. 2. The molecular representation of the eumelanin (MNPs), hydrophilic glycol chitosan (HGC), and cisplatin (CDDP) (a) ATR-FTIR (b) and thermogravimetric spectra (c) of HGC/CDDP-MNPs, HGC/MNPs, CDDP-MNPs nanocomplexes, and MNPs, HGC, and CDDP powders.

about 98%. On the other hand, the weight loss of natural melanin nanoparticles took place in two steps. The first degradation step was observed between 34 °C and 224 °C, corresponding to the loss of free water and/or bound water in melanin equivalent to around 15% of the total mass. The second thermal decomposition started at 224 °C as CO_2 was evaporated. Although TGA analyses were carried out up to 600 °C, only about 51% of the initial melanin mass was lost at this temperature range suggesting good thermal stability of melanin due to its graphite-like structure [62]. Hydrophilic glycol chitosan exhibited three-step weight loss at 70 °C, 280 °C, and 538 °C. The initial weight decrement

indicates the loss of (un)bound water, whereas the second corresponds to the chitosan backbone's thermal degradation [63], and the total char yield was 35%. The intra- and inter-molecular hydrogen bonds within the MNP and HGC structures make them highly thermal stable. However, upon nanohybrid formation, the initial degradation temperatures decreased for the MNP composites (HGC/MNPs, CDDP-MNPs, and HGC/CDDP-MNPs). This decrement indicates the weakening of hydrogen bonds in MNP and HGC because of the possibly formed interactions between the components. This suggests that compatibility between drug/coating material and nanoparticles aligns with the ATR-FTIR analyses.

3.3. Drug loading capacity and entrapment efficiency

Drug loading and entrapment efficiency depend on drug solubility, drug affinity with the nanoparticles, and the nanocomplex production process. Although a limited number of studies were conducted using natural MNPs as drug nanocarriers, we can state that with the herein presented work, we successfully enhanced both entrapment efficiency and loading capacity of the natural MNPs compared to previously published studies [41,42]. The drug entrapment efficiency and loading capacity of MNPs were calculated as 93.2% ± 2.0 and 21.7% ± 0.5 for the CDDP-MNPs. The HGC modification did not affect encapsulation efficiency or loading capacity (94.9% ± 1.1 and 24.7% ± 0.4) as expected. This is because the surface coating process was performed immediately following CDDP loading into MNPs and the removal of unloaded drugs by washing and centrifugation.

3.4. In vitro drug release

The release profiles of CDDP from CDDP-MNPs and HGC/CDDP-MNPs matrices were obtained at the predetermined time points from 1 to 264 h via UV–vis spectrophotometric measurements after incubating these nanoformulations in a physiological buffer solution (PBS, pH: 7.4). The release behavior was examined by plotting the data obtained from *in vitro* drug release studies as the cumulative amount of drug released (%) versus time (Fig. 3). According to the release profiles of CDDP-MNPs and HGC/CDDP-MNPs, three types of release behaviors were seen (Fig. 3a). In the first region (1–6 h), the rate of drug delivery was controlled by the swelling and osmotic pressure differences for HGC/CDDP-MNPs. The polymer relaxation occurs as the HGC absorbs buffer solution while osmotic pressure differences regulate swelling [64]. Such swelling behavior is highly preferred to obtain a controllable solute release through modulating the swelling ratio by simply adjusting the physicochemical features of the nanocarrier. However, for MNP-CDDPs, only the concentration gradients dominate for the CDDP release due to the non-swellable and non-erodible nature, which explains the difference between the released CDPP amounts for each nanoformulation.

The second phase of the release curves (6–24 h for both CDDP-MNPs and HGC/CDDP-MNPs) showed a sustained release up to 24 h until the lag period began (24–264 h) (Fig. 3b). The sustained release behavior can be explained by the π-π stacking interaction that causes firm contact between aromatic rings in CDDP and MNPs [42]. In addition, the TGA and ATR-FTIR analyses indicated compatibility between MNPs and CDDP and HGC and CDDP; hence slower release of the drug from the CDDP-MNPs and the HGC/CDDP-MNPs nanocomplexes can be explained. Moreover, 30% and 36% of CDDP remained unreleased at the 264th h for CDDP-MNPs and HGC/CDDP-MNPs, which the hydrogen bonding can describe.

For kinetic model analyses, the in *vitro* drug release data were fitted into four different kinetic models explained in the Supporting *Information* document with the data obtained from the respected equations (**Table S1**). The best fitted kinetic models describing CDDP release from CDDP-MNPs and HGC/CDDP-MNPs were determined by considering the highest coefficient of determination (R^2) obtained. It was found that the time course release data for both nanoformulations were best fitted with

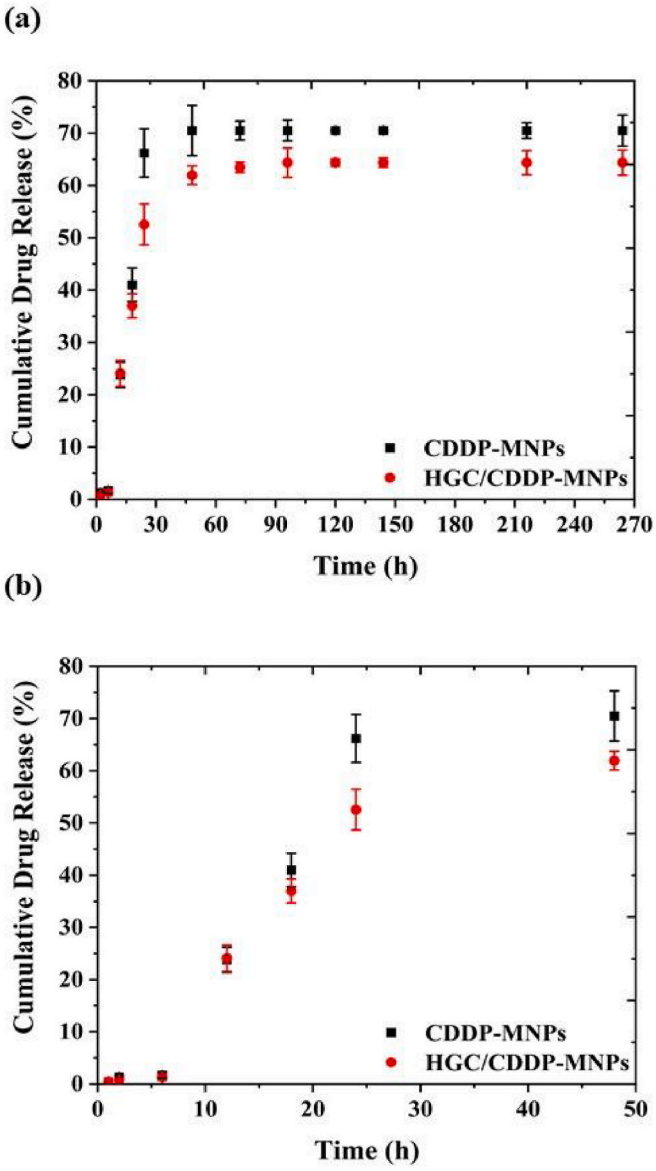

Fig. 3. The cumulative released drug amount (%) from CDDP-MNPs and HGC/CDDP-MNPs matrices versus time. Time course data are given in full range (a) and for the first 48 h (b).

the Korsmeyer-Peppas model; the diffusional exponents (n) were calculated as 0.89 and 0.97 for CDDP-MNPs and HGC/CDDP-MNPs, indicative of Super Case II Transport (n > 0.89). Although melanin is known to be a non-swellable and erodible material in physiological buffer [28], hydrophilic chitosan coating would have altered the resultant physicochemical properties, notably upon physiological buffer uptake. Therefore, the release of the CDDPs from HGC/CDDP-MNPs was dominated by molecular polymer relaxation of the HGC polymeric chain and swelling. In contrast, in the CDDP-MNPs case, only osmotic forces were taking place [64].

3.5. In vitro cell viability assay

Huh7 cells are a well-established and differentiated hepatocyte-derived cellular carcinoma cell line, where CDDP is widely used for chemotherapeutic treatment [65]. In this work, Huh7 cells were exposed to both nanocomplex-bound CDDPs and free CDDP for 72 h to evaluate the effect of produced nanoformulations compared to free CDPP. Ultimately, an MTT assay was performed to assess cell viability,

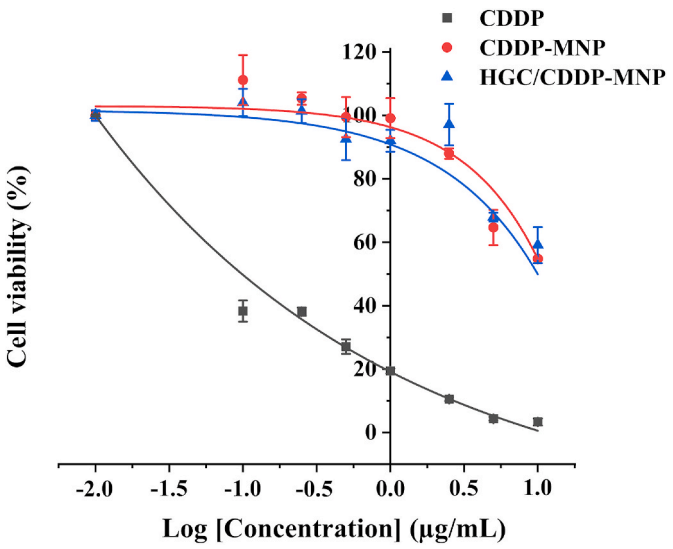

Fig. 4. Drug concentration and formulation influence on cell viability obtained for free CDDPs and the CDDP-loaded nanoformulations (CDDP-MNPs and HGC/CDDP-MNPs) (n 3).

proliferation as well as cytotoxicity, and the obtained data are sketched in Fig. 4 and Fig. S2 (given in Supplementary Materials).

A drug response curve was generated after 72 h of treatment with each formulation: free CDDP, CDDP-MNPs, and HGC/CDDP-MNPs. IC_{50} values for CDDP-MNPs and HGC/CDDP-MNPs were calculated as 10.25 μg/mL and 13.03 μg/mL, respectively. The higher IC_{50} values obtained for CDDP-MNPs and HGC/CDDP-MNPs nanoformulations correlated to the sustained release behaviors of nanocarrier-bound CDDPs while inhibiting the proliferation of Huh7 cells. On the other hand, IC_{50} for CDDP was 0.11 μg/mL, suggesting that when free dosage format CDDP are utilized for chemotherapy, they yield much higher cytotoxicity even at ng/mL concentration level than its herein proposed nanoformulations, which also lines up with the previous findings [6,38,66].

4. Conclusion

In this work, we presented a eumelanin-based nanocomplex as an alternative chemotherapeutic agent for highly cytotoxic free liquid dosage format cisplatin that is widely applied in clinics for several cancer treatments. Cisplatin could be easily conjugated with melanin nanocarrier through single-step mixing. The resultant nanocomplexes showed high drug loading/entrapment performance, which also exhibited sustained release obeying Super Case II Transport, as confirmed *in vitro*. The cell viability results demonstrated that the CDDP-loaded nanocarriers showed distinctly higher IC_{50} values than the free CDDP, fulfilling low dosage requirements while sustainably destroying liver cancer cells, as expected from a promising controlled release system for the formulation of nanomedicine. The approach we undertook in this study with MNPs and HGC/MNPs could be exploited further for cellular organelle and junction targeting. Interestingly, melanin-like and chitosan comprising nanoparticles were shown to be instrumental in mitochondrial targeting [67,68] and/or cell-cell junction modulation [69].

In the future, these nanoparticles will be investigated *in vivo* for their targeting capability and effectiveness. Additionally, the effect of other biocompatible and biodegradable materials like nanostructured lipid carriers, mesoporous silica on drug delivery and cell viability could be evaluated [70–72]. Additionally, it is noteworthy to mention that melanin nanoparticles can show photothermal behavior under light irradiation [73,74] and may act as MRI contrast agents, which facilitates imaging of cancer sites and therapy simultaneously. Recently, Yan et al. were conducted a tremendous study for the preparation of C60-decorated natural melanin nanoparticles conjugated with hyaluronic acid and to monitor the effectiveness of their multimodal treatment strategy including photodynamic therapy, photothermal therapy and immunotherapy [75]. Several studies have investigated hyaluronic acid modified carriers for active targeting of tumor cells and discriminating tumor cells from healthy cells since hyaluronic acid is the primary CD44 binding molecule [75–80]. These CD44 receptors highly expressed on tumor cell membranes and can allow nanoparticles to enter cells through phagocytosis. Therefore, application adaptability by evaluating of synergistic effect of hyaluronic acid modified proposed nanocomplex for such a combinatory theragnostic approach may constitute a hopeful strategy for future applications in liver cancer cells.

Author contributions

The manuscript was written with the contributions of all authors. All authors have approved the final version of the manuscript.

Notes

The authors declare no competing financial interest.

Author statement

Aleyna Atik: Conceptualization, Methodology, Investigation, Visualization, Writing- Original draft preparation. **Tuğçe Günal:** Conceptualization, Methodology, Investigation, Writing- Original draft preparation. **Sıla Naz Köse:** Investigation. **Burcak Alp:** Investigation, Writing- Reviewing and Editing. **Cihangir Yandım:** Investigation, Writing- Reviewing and Editing. **Mete Kaleli:** Resources, Formal analysis, Writing- Original draft preparation. **Pınar Acar Bozkurt:** Resources, Writing- Reviewing and Editing. **Gözde Kabay:** Conceptualization, Methodology, Visualization, Writing- Reviewing and Editing, Supervision. **Gizem Kaleli-Can:** Conceptualization, Methodology, Visualization, Investigation, Resources, Writing- Reviewing and Editing, Supervision, Project Administration.

Declaration of competing interest

The authors declare that they have no known competing financial interests or personal relationships that could have appeared to influence the work reported in this paper.

Data availability

Data will be made available on request.

Abbreviations

ATR-FTIR	Attenuated total reflectance-Fourier transform infrared spectroscopy
CDDP	Cisplatin
DIW	Deionized water
DMF	dimethylformamide
HGC	Hydrophilic Glycol Chitosan
SEM	Scanning electron microscopy
MNP	Natural Melanin Nanoparticle
OPDA	o-phenylenediamine
TGA	Thermal gravimetric analysis
MTT	3-(4,5-Dimethylthiazol-2-yl)-2,5-Diphenyltetrazolium Bromide

References

[1] International Agency for Research on Cancer (IARC), Estimated number of new cases from 2020 to 2040, Cancer Tomorrow, https://gco.iarc.fr/tomorrow/en/dataviz/isotype?types=0&single_unit=500000. (Accessed 10 June 2022).

[2] D.T. Debela, S.G. Muzazu, K.D. Heraro, M.T. Ndalama, B.W. Mesele, D.C. Haile, S. K. Kitui, T. Manyazewal, New approaches and procedures for cancer treatment: current perspectives, SAGE Open Med. 9 (2021), 205031212110343, https://doi.org/10.1177/20503121211034366.

[3] M.A. Moses, H. Brem, R. Langer, Advancing the field of drug delivery: taking aim at cancer, Cancer Cell 4 (5) (2003) 337–341, https://doi.org/10.1016/S1535-6108(03)00276-9.

[4] S. Ghosh, Cisplatin: the first metal based anticancer drug, Bioorg. Chem. 88 (2019), https://doi.org/10.1016/J.BIOORG.2019.102925.

[5] N. Martinho, T.C.B. Santos, H.F. Florindo, L.C. Silva, Cisplatin-membrane interactions and their influence on platinum complexes activity and toxicity, Front. Physiol. 9 (JAN) (2018), https://doi.org/10.3389/FPHYS.2018.01898.

[6] X. Duan, C. He, S.J. Kron, W. Lin, Nanoparticle formulations of cisplatin for cancer therapy, Wiley Interdiscip. Rev. Nanomed. Nanobiotechnol. 8 (5) (2016) 776–791, https://doi.org/10.1002/WNAN.1390.

[7] S. Dasari, P. Bernard Tchounwou, Cisplatin in cancer therapy: molecular mechanisms of action, Eur. J. Pharmacol. 740 (2014) 364, https://doi.org/10.1016/J.EJPHAR.2014.07.025.

[8] H. Wang, S. Guo, S.J. Kim, F. Shao, J.W. Kei Ho, K.U. Wong, Z. Miao, D. Hao, M. Zhao, J. Xu, J. Zeng, K.H. Wong, L. Di, A.H.H. Wong, X. Xu, C.X. Deng, Cisplatin prevents breast cancer metastasis through blocking early EMT and retards cancer growth together with paclitaxel, Theranostics 11 (5) (2021) 2442–2459, https://doi.org/10.7150/THNO.46460.

[9] Cisplatin (intravenous route) side effects - mayo clinic. https://www.mayoclinic.org/drugs-supplements/cisplatin-intravenous-route/side-effects/drg-20062953?p=1. (Accessed 11 June 2022).

[10] Chemotherapy side effects | American cancer society. https://www.cancer.org/treatment/treatments-and-side-effects/treatment-types/chemotherapy/chemotherapy-side-effects.html. (Accessed 11 June 2022).

[11] R.P. Miller, R.K. Tadagavadi, G. Ramesh, W.B. Reeves, Mechanisms of cisplatin nephrotoxicity, Toxins 2 (11) (2010) 2490, https://doi.org/10.3390/TOXINS2112490.

[12] M. Waseem, M. Bhardwaj, H. Tabassum, S. Raisuddin, S. Parvez, Cisplatin hepatotoxicity mediated by mitochondrial stress, Drug Chem. Toxicol. 38 (4) (2015) 452–459, https://doi.org/10.3109/01480545.2014.992437.

[13] L. Cao, Y. Zhu, W. Wang, G. Wang, S. Zhang, H. Cheng, Emerging nano-based strategies against drug resistance in tumor chemotherapy, Front. Bioeng. Biotechnol. 9 (2021) 1255, https://doi.org/10.3389/FBIOE.2021.798882/BIBTEX.

[14] X. Xu, W. Ho, X. Zhang, N. Bertrand, O. Farokhzad, Cancer nanomedicine: from targeted delivery to combination therapy, Trends Mol. Med. 21 (4) (2015) 223–232, https://doi.org/10.1016/j.molmed.2015.01.001.

[15] Y.S. Zhang, A. Khademhosseini, Seeking the right context for evaluating nanomedicine: from tissue models in petri dishes to microfluidic organs-on-a-chip, Nanomedicine 10 (5) (2015) 685–688, https://doi.org/10.2217/nnm.15.18.

[16] B. Theek, L.Y. Rizzo, J. Ehling, F. Kiessling, T. Lammers, The theranostic path to personalized nanomedicine, Clin. Trans. Imag. 2 (1) (2014) 67–76, https://doi.org/10.1007/s40336-014-0051-5.

[17] P. Hunziker, Nanomedicine - shaping the medicine of the future, *Zeitschrift fur Medizinische Physik*. February (2012) 1–3, https://doi.org/10.1016/j.zemedi.2011.11.001.

[18] M.G. Krukemeyer, V. Krenn, F. Huebner, W. Wagner, R. Resch, History and possible uses of nanomedicine based on nanoparticles and nanotechnological progress, J. Nanomed. Nanotechnol. 6 (6) (2015) 336, https://doi.org/10.4172/2157-7439.1000336.

[19] J.I. Hare, T. Lammers, M.B. Ashford, S. Puri, G. Storm, S.T. Barry, Challenges and strategies in anti-cancer nanomedicine development: an industry perspective, Adv. Drug Deliv. Rev. 108 (2017) 25–38, https://doi.org/10.1016/j.addr.2016.04.025.

[20] F. Rommasi, N. Esfandiari, Liposomal nanomedicine: applications for drug delivery in cancer therapy, Nanoscale Res. Lett. 16 (1) (2021) 1–20, https://doi.org/10.1186/S11671-021-03553-8.

[21] O.A. Kuchur, S.A. Tsymbal, M.V. Shestovskaya, N.S. Serov, M.S. Dukhinova, A. A. Shtil, Metal-derived nanoparticles in tumor theranostics: potential and limitations, J. Inorg. Biochem. 209 (2020), 111117, https://doi.org/10.1016/j.jinorgbio.2020.111117.

[22] L. Degli Esposti, F. Carella, M. Iafisco, Inorganic nanoparticles for theranostic use, in: Electrofluidodynamic Technologies (EFDTs) for Biomaterials and Medical Devices, Elsevier, 2018, pp. 351–376, https://doi.org/10.1016/B978-0-08-101745-6.00017-7.

[23] D. Singh, S. Singh, J. Sahu, S. Srivastava, Manju, R. Singh, Ceramic nanoparticles: recompense, cellular uptake and toxicity concerns, Nanomed. Biotechnol. 44 (1) (2016) 401–409, https://doi.org/10.3109/21691401.2014.955106.

[24] C.G. Qian, Y.L. Chen, P.J. Feng, X.Z. Xiao, M. Dong, J.C. Yu, Q.Y. Hu, Q.D. Shen, Z. Gu, Conjugated polymer nanomaterials for theranostics, *Acta Pharmacologica Sinica*. Nature Publishing Group June 1 (2017) 764–781, https://doi.org/10.1038/aps.2017.42.

[25] H. Peng, X. Liu, G. Wang, M. Li, K.M. Bratlie, E. Cochran, Q. Wang, Polymeric multifunctional nanomaterials for theranostics, J. Mater. Chem. B 3 (34) (2015) 6856–6870, https://doi.org/10.1039/C5TB00617A.

[26] S.K. Nitta, K. Numata, Biopolymer-based nanoparticles for drug/gene delivery and tissue engineering, Int. J. Mol. Sci. 14 (1) (2013) 1629, https://doi.org/10.3390/IJMS14011629.

[27] A.A. Vodyashkin, P. Kezimana, A.A. Vetcher, Y.M. Stanishevskiy, Biopolymeric nanoparticles–multifunctional materials of the future, Polymers 14 (11) (2022) 2287, https://doi.org/10.3390/POLYM14112287.

[28] B. Ozlu, G. Kabay, I. Bocek, M. Yilmaz, A.K. Piskin, B.S. Shim, M. Mutlu, Controlled release of doxorubicin from polyethylene glycol functionalized melanin nanoparticles for breast cancer therapy: Part I. Production and drug release performance of the melanin nanoparticles, Int. J. Pharm. 570 (2019), https://doi.org/10.1016/j.ijpharm.2019.118613.

[29] T. Eom, K. Woo, B.S. Shim, Melanin: a naturally existing multifunctional material, Appl. Chem. Eng. 27 (2) (2016) 115–122, https://doi.org/10.14478/ace.2016.1029.

[30] T. Eom, K. Woo, W. Cho, J.E. Heo, D. Jang, J.I. Shin, D.C. Martin, J.J. Wie, B. S. Shim, Nanoarchitecturing of natural melanin nanospheres by layer-by-layer assembly: macroscale anti-inflammatory conductive coatings with optoelectronic tunability, Biomacromolecules 18 (6) (2017) 1908–1917, https://doi.org/10.1021/acs.biomac.7b00336.

[31] M. Rozanowska, T. Sarna, E.J. Land, T.G. Truscott, Free radical scavenging properties of melanin. Interaction of Eu and pheo melanin models with reducing and oxidizing agents, Free Radic. Biol. Med. 26 (98) (1999) 518–525.

[32] T. Sun, D. Jiang, Z.T. Rosenkrans, E.B. Ehlerding, D. Ni, C. Qi, C.J. Kutyreff, T. E. Barnhart, J.W. Engle, P. Huang, W. Cai, A melanin-based natural antioxidant defense nanosystem for theranostic application in acute kidney injury, Adv. Funct. Mater. 29 (48) (2019), 1904833, https://doi.org/10.1002/adfm.201904833.

[33] X. Fu, M. Xie, M. Lu, L. Shi, T. Shi, M. Yu, Characterization of the physicochemical properties, antioxidant activity, and antiproliferative activity of natural melanin from S. Reiliana, Sci. Rep. 12 (1) (2022) 2110, https://doi.org/10.1038/s41598-022-05676-z.

[34] G. Kaleli-Can, B. Ozlu, H.F. Özgüzar, B. Onal-Ulusoy, G. Kabay, T. Eom, B.S. Shim, M. Mutlu, Natural melanin nanoparticle-decorated screen-printed carbon electrode: performance test for amperometric determination of hexavalent chromium as model trace, Electroanalysis 32 (8) (2020) 1696–1706, https://doi.org/10.1002/elan.202000038.

[35] Q. Jiang, Z. Luo, Y. Men, P. Yang, H. Peng, R. Guo, Y. Tian, Z. Pang, W. Yang, Red blood cell membrane-camouflaged melanin nanoparticles for enhanced photothermal therapy, Biomaterials 143 (2017) 29–45, https://doi.org/10.1016/j.biomaterials.2017.07.027.

[36] G. Kabay, A.E. Meydan, T. Eom, B.S. Shim, M. Mutlu, G. Kaleli-Can, Stimuli-responsive nanoparticle-nanofiber hybrids for drug delivery and photodynamic therapy, Int. J. Pharm. 630 (2023), 122442, https://doi.org/10.1016/j.ijpharm.2022.122442.

[37] H. Liu, Y. Yang, Y. Liu, J. Pan, J. Wang, F. Man, W. Zhang, G. Liu, Melanin-like nanomaterials for advanced biomedical applications: a versatile platform with extraordinary promise, Adv. Sci. 2020 7 (7) (2020), 1903129, https://doi.org/10.1002/advs.201903129.

[38] J.H. Kim, Y.S. Kim, K. Park, S. Lee, H.Y. Nam, K.H. Min, H.G. Jo, J.H. Park, K. Choi, S.Y. Jeong, R.W. Park, I.S. Kim, K. Kim, I.C. Kwon, Antitumor efficacy of cisplatin-loaded glycol chitosan nanoparticles in tumor-bearing mice, J. Contr. Release 127 (1) (2008) 41–49, https://doi.org/10.1016/J.JCONREL.2007.12.014.

[39] I.C. Sun, J.H. Na, S.Y. Jeong, D.E. Kim, I.C. Kwon, K. Choi, C. Ahn, K. Kim, Biocompatible glycol chitosan-coated gold nanoparticles for tumor-targeting CT imaging, Pharmaceut. Res. 31 (6) (2014) 1418–1425, https://doi.org/10.1007/s11095-013-1142-0.

[40] L. Yan, S.H. Crayton, J.P. Thawani, A. Amirshaghaghi, A. Tsourkas, Z. Cheng, A pH-responsive drug-delivery platform based on glycol chitosan–coated liposomes, Small 11 (37) (2015) 4870–4874, https://doi.org/10.1002/smll.201501412.

[41] M. Araújo, R. Viveiros, T.R. Correia, I.J. Correia, V.D.B. Bonifácio, T. Casimiro, A. Aguiar-Ricardo, Natural melanin: a potential PH-responsive drug release device, Int. J. Pharm. 469 (1) (2014) 140–145, https://doi.org/10.1016/J.IJPHARM.2014.04.051.

[42] R. Zhang, Q. Fan, M. Yang, K. Cheng, X. Lu, L. Zhang, W. Huang, Z. Cheng, Engineering melanin nanoparticles as an efficient drug–delivery system for imaging-guided chemotherapy, Adv. Mater. 27 (34) (2015) 5063–5069, https://doi.org/10.1002/ADMA.201502201.

[43] P. Jakubiak, P. Jakubiak, C. Cantrill, A. Urtti, A. Urtti, R. Alvarez-Sánchez, Establishment of an in vitro-in vivo correlation for melanin binding and the extension of the ocular half-life of small-molecule drugs, Mol. Pharm. 16 (12) (2019) 4890–4901, https://doi.org/10.1021/ACS.MOLPHARMACEUT.9B00769.

[44] S. Roy, L. van Hai, H.C. Kim, L. Zhai, J. Kim, Preparation and characterization of synthetic melanin-like nanoparticles reinforced chitosan nanocomposite films, Carbohydr. Polym. 231 (2020), https://doi.org/10.1016/J.CARBPOL.2019.115729.

[45] M. Basotra, S.K. Singh, M. Gulati, Development and validation of a simple and sensitive spectrometric method for estimation of cisplatin hydrochloride in tablet dosage forms: application to dissolution studies, ISRN Anal.Chem. 2013 (2013) 1–8, https://doi.org/10.1155/2013/936254.

[46] S. Dash, P.N. Murthy, L. Nath, P. Chowdhury, Kinetic modeling on drug release from controlled drug delivery systems, Acta Pol. Pharm. 67 (3) (2010) 217–223.

[47] Mathematical models of drug release, in: Strategies to Modify the Drug Release from Pharmaceutical Systems, Woodhead Publishing, 2015, pp. 63–86, https://doi.org/10.1016/B978-0-08-100092-2.00005-9.

[48] J. van Meerloo, G.J.L. Kaspers, J. Cloos, Cell sensitivity assays: the MTT assay, Methods Mol. Biol. 731 (2011) 237–245, https://doi.org/10.1007/978-1-61779-080-5_20.

[49] J. Jiang, G. Oberdörster, P. Biswas, Characterization of size, surface charge, and agglomeration state of nanoparticle dispersions for toxicological studies,

J. Nanoparticle Res. 11 (1) (2008) 77–89, https://doi.org/10.1007/S11051-008-9446-4.
[50] M.v. Baranov, M. Kumar, S. Sacanna, S. Thutupalli, G. van den Bogaart, Modulation of immune responses by particle size and shape, Front. Immunol. 11 (2021), https://doi.org/10.3389/FIMMU.2020.607945/FULL.
[51] H. Kobayashi, R. Watanabe, P.L. Choyke, Improving conventional enhanced permeability and retention (EPR) effects; what is the appropriate target? Theranostics 4 (1) (2013) 81–89, https://doi.org/10.7150/THNO.7193.
[52] X.Y. Wong, A. Sena-Torralba, R. Álvarez-Diduk, K. Muthoosamy, A. Merkoçi, Nanomaterials for nanotheranostics: tuning their properties according to disease needs, ACS Nano 14 (3) (2020) 2585–2627, https://doi.org/10.1021/acsnano.9b08133.
[53] D. Chenthamara, S. Subramaniam, S.G. Ramakrishnan, S. Krishnaswamy, M. M. Essa, F.H. Lin, M.W. Qoronfleh, Therapeutic efficacy of nanoparticles and routes of administration, Biomater. Res. 23 (1) (2019) 1–29, https://doi.org/10.1186/S40824-019-0166-X.
[54] S.D. Allison, Analysis of initial burst in PLGA microparticles, Expet Opin. Drug Deliv. 5 (6) (2008) 615–628, https://doi.org/10.1517/17425247.5.6.615.
[55] Q. Li, J. Zhou, L. Zhang, Structure and properties of the nanocomposite films of chitosan reinforced with cellulose whiskers, J. Polym. Sci. B Polym. Phys. 47 (11) (2009) 1069–1077, https://doi.org/10.1002/POLB.21711.
[56] S. Roy, J.W. Rhim, Preparation of carbohydrate-based functional composite films incorporated with curcumin, Food Hydrocolloids 98 (2020), 105302, https://doi.org/10.1016/J.FOODHYD.2019.105302.
[57] A.A.P. Mansur, H.S. Mansur, Quantum dot/glycol chitosan fluorescent nanoconjugates, Nanoscale Res. Lett. 10 (1) (2015), https://doi.org/10.1186/S11671-015-0879-2.
[58] A. Mavridi-Printezi, M. Guernelli, A. Menichetti, M. Montalti, Bio-applications of multifunctional melanin nanoparticles: from nanomedicine to nanocosmetics, Nanomaterials 10 (11) (2020) 2276, https://doi.org/10.3390/NANO10112276.
[59] G.J. Kirkpatrick, J.A. Plumb, O.B. Sutcliffe, D.J. Flint, N.J. Wheate, Evaluation of anionic half generation 3.5–6.5 poly (amidoamine) dendrimers as delivery vehicles for the active component of the anticancer drug cisplatin, J. Inorg. Biochem. 105 (9) (2011) 1115–1122, https://doi.org/10.1016/j.jinorgbio.2011.05.017.
[60] H. Nguyen, N.H. Nguyen, N.Q. Tran, C.K. Nguyen, Improved method for preparing cisplatin-dendrimer nanocomplex and its behavior against NCI-H460 lung cancer cell, J. Nanosci. Nanotechnol. 15 (6) (2015) 4106–4110, https://doi.org/10.1166/jnn.2015.9808.
[61] N.A.N. Tong, T.P. Nguyen, N. Cuu Khoa, N.Q. Tran, Aquated cisplatin and heparin-pluronic nanocomplexes exhibiting sustainable release of active platinum compound and NCI-H460 lung cancer cell antiproliferation, J. Biomater. Sci. Polym. Ed. 27 (8) (2016) 709–720, https://doi.org/10.1080/09205063.2016.1154239.
[62] S.N. Dezidério, C.A. Brunello, M.I.N. da Silva, M.A. Cotta, C.F.O. Graeff, Thin films of synthetic melanin, J. Non-Cryst. Solids 338–340 (1 SPEC. ISS.) (2004) 634–638, https://doi.org/10.1016/J.JNONCRYSOL.2004.03.058.
[63] R.K. Mishra, S. Mondal, M. Datt, A.K. Banthia, Development and characterization of chitosan and phosphomolybdic acid (PMA) based composites, Int. J. Plastics Technol. 14 (1) (2010) 80–92, https://doi.org/10.1007/S12588-009-0018-Y.
[64] C.S. Brazel, N.A. Peppas, Mechanisms of solute and drug Transport in relaxing, swellable, hydrophilic glassy polymers, Polymer 40 (12) (1999) 3383–3398, https://doi.org/10.1016/S0032-3861(98)00546-1.
[65] T. Ishikawa, Future perspectives on the treatment of hepatocellular carcinoma with cisplatin, World J. Hepatol. 1 (1) (2009) 8, https://doi.org/10.4254/WJH.V1.I1.8.
[66] T. Wakamatsu, Y. Nakahashi, D. Hachimine, T. Seki, K. Okazaki, The combination of glycyrrhizin and lamivudine can reverse the cisplatin resistance in hepatocellular carcinoma cells through inhibition of multidrug resistance-associated proteins, Int. J. Oncol. 31 (6) (2007) 1465–1472, https://doi.org/10.3892/IJO.31.6.1465/HTML.
[67] W.Q. Li, Z. Wang, S. Hao, H. He, Y. Wan, C. Zhu, S.Y. Zheng, Mitochondria-targeting polydopamine nanoparticles to deliver doxorubicin for overcoming drug resistance, ACS Appl. Mater. Interfaces 9 (20) (2017) 16793–16802, https://doi.org/10.1021/acsami.7b01540.
[68] S. Mallick, S.J. Song, Y. Bae, J.S. Choi, Self-assembled nanoparticles composed of glycol chitosan-dequalinium for mitochondria-targeted drug delivery, Int. J. Biol. Macromol. 132 (2019) 451–460, https://doi.org/10.1016/j.ijbiomac.2019.03.215.
[69] T.H. Yeh, L.W. Hsu, M.T. Tseng, P.L. Lee, K. Sonjae, Y.C. Ho, H.W. Sung, Mechanism and consequence of chitosan-mediated reversible epithelial tight junction opening, Biomaterials 32 (26) (2011) 6164–6173, https://doi.org/10.1016/j.biomaterials.2011.03.056.
[70] E. Ahmadian, A. Eftekhari, T. Kavetskyy, A.Y. Khosroushahi, V.A. Turksoy, R. Khalilov, Effects of quercetin loaded nanostructured lipid carriers on the paraquat-induced toxicity in human lymphocytes, Pestic. Biochem. Physiol. 167 (2020), 104586, https://doi.org/10.1016/j.pestbp.2020.104586.
[71] A. Hasanzadeh, B. Gholipour, S. Rostamnia, A. Eftekhari, A. Tanomand, S. Khaksar, R. Khalilov, Biosynthesis of AgNPs onto the urea-based periodic mesoporous organosilica (AgxNPs/Ur-PMO) for antibacterial and cell viability assay, J. Colloid Interface Sci. 585 (2021) 676–683, https://doi.org/10.1016/j.jcis.2020.10.047.
[72] Y. Zhang, Q. Wang, Y. Ji, L. Fan, B. Ding, J. Lin, L. Wang, Mitochondrial targeted melanin@ mSiO2 yolk-shell nanostructures for NIR-II-driven photo-thermal-dynamic/immunotherapy, Chem. Eng. J. 435 (2022), 134869, https://doi.org/10.1016/j.cej.2022.134869.
[73] B. Akman, B. İslam, G.K. Can, N.T. Avşar, D.Ş. Karaman, E. Baysoy, Gıda ve sağlık uygulamaları İçin UV-A Işıma Altında Alternatif Bir Fotokatalizör Olarak: doğal melanin Nanoparçacıkları, Avrupa Bilim ve Teknoloji Dergisi (32) (2021) 940–946, https://doi.org/10.31590/ejosat.1040830.
[74] B. Akman, B. İslam, G. Kaleli-Can, E. Baysoy, N. Topaloğlu, D.Ş. Karaman, The protective role of natural melanin nanoparticles under UVC exposure, in: 2021 Medical Technologies Congress (TIPTEKNO), IEEE, 2021, pp. 1–4, https://doi.org/10.1109/TIPTEKNO53239.2021.9633009.
[75] J.H. Yan, Y.S. Ji, M.L. Yang, J. Fu, H. Shan, L.L. Wang, J.S. Shi, C60-Decorated melanin nanoparticles conjugated with hyaluronic acid for synergistic theranostic and immunotherapy of tumors under near-infrared excitation, ACS Appl. Nano Mater. 3 (9) (2020) 8817–8828, https://doi.org/10.1021/acsanm.0c01607.
[76] G. Mattheolabakis, L. Milane, A. Singh, M.M. Amiji, Hyaluronic acid targeting of CD44 for cancer therapy: from receptor biology to nanomedicine, J. Drug Target. 23 (7–8) (2015) 605–618, https://doi.org/10.3109/1061186X.2015.1052072.
[77] A.D. Wojcicki, H. Hillaireau, T.L. Nascimento, S. Arpicco, M. Taverna, S. Ribes, E. Fattal, Hyaluronic acid-bearing lipoplexes: physico-chemical characterization and in vitro targeting of the CD44 receptor, J. Contr. Release 162 (3) (2012) 545–552, https://doi.org/10.1016/j.jconrel.2012.07.015.
[78] S. Ganesh, A.K. Iyer, F. Gattacceca, D.V. Morrissey, M.M. Amiji, In vivo biodistribution of siRNA and cisplatin administered using CD44-targeted hyaluronic acid nanoparticles, J. Contr. Release 172 (3) (2013) 699–706, https://doi.org/10.1016/j.jconrel.2013.10.016.
[79] T. Yu, Y. Li, X. Gu, Q. Li, Development of a hyaluronic acid-based nanocarrier incorporating doxorubicin and cisplatin as a pH-sensitive and CD44-targeted anti-breast cancer drug delivery system, Front. Pharmacol. 11 (2020), 532457, https://doi.org/10.3389/fphar.2020.532457.
[80] N. Alam, M. Koul, M.J. Mintoo, V. Khare, R. Gupta, N. Rawat, P.N. Gupta, Development and characterization of hyaluronic acid modified PLGA based nanoparticles for improved efficacy of cisplatin in solid tumor, Biomed. Pharmacother. 95 (2017) 856–864, https://doi.org/10.1016/j.biopha.2017.08.108.